Remote Sensing of Environment 112 (2008) 3668–3679

Contents lists available at ScienceDirect

Remote Sensing of Environment

journal homepage: www.elsevier.com/locate/rse

Regional mapping of human settlements in southeastern China with multisensor remotely sensed data

Dengsheng Lu [a,*], Hanqin Tian [a], Guomo Zhou [b], Hongli Ge [b]

[a] School of Forestry and Wildlife Sciences, Auburn University, 602 Duncan Drive, Auburn, AL 36849, USA
[b] School of Environmental Technology, Zhejiang Forestry University, Lin'An, Zhejiang, China

ARTICLE INFO

Article history:
Received 6 November 2007
Received in revised form 16 May 2008
Accepted 24 May 2008

Keywords:
Human settlements
Regional mapping
ETM+
MODIS NDVI
DMSP-OLS
Partial unmixing
Regression model
Southeastern China

ABSTRACT

Mapping human settlements from remotely sensed data at regional and global scales has attracted increasingly attention but remains a challenge. The thresholding technique is a common approach for settlement mapping based on the DMSP-OLS data. However, this approach often omits the areas with small proportional settlements such as towns and villages and overestimates urban extents, resulting in information loss of spatial patterns. This paper explored an integrated approach based on a combined use of multiple remotely sensed data to map settlements in southeastern China. Human settlements for selected sites were mapped from Landsat ETM+ images with a hybrid approach and they were used as reference data. The DMSP-OLS and Terra MODIS NDVI data were combined to develop a settlement index image. This index image was used to map a pixel-based settlement image with expert rules. A regression model was established to estimate fractional settlements at the regional scale, which the DMSP-OLS and MODIS NDVI data were used as independent variables and the settlement data derived from ETM+ images were used as a dependent variable. This research indicated that a combination of DMSP-OLS and NDVI variables provided a better estimation performance than single DMSP-OLS or NDVI variable, and the integrated approach for settlement mapping at the regional scale was promising. Compared to the results from the traditional thresholding technique, the estimated fractional settlement image in this paper greatly improved the spatial patterns of settlement distribution and accuracy of settlement areas. This paper provided a rapid and accurate approach to estimate fractional settlements from coarse spatial resolution images at the regional scale by combining a limited number of medium spatial resolution images. This research is especially valuable for timely updating settlement databases at regional and global scales with limited time, labor, and cost.

1. Introduction

Human settlements are the places where human beings live, work, and recreate, including cities, towns, and villages (Ridd & Hipple, 2006). The size, pattern, and spatial distribution of human settlements are a fundamental data source for evaluating impacts of urbanization on environments and for urban management and planning (Milesi et al., 2003a; Pauleit et al., 2005). Human settlements are also closely related to population distribution and economic growth, thus they are an important data source for demographic–economic related studies (Meyer & Turner, 1992). With increasing pressure of population and economic growth, the conversion rate of vegetation or agricultural lands to human settlements has been increased sharply during past decades, especially in developing countries such as China (Liu et al., 2005a,b). The urbanization causing many environmental problems, such as vegetation loss, air pollution, water shortage and contamination, and urban heat island, has been recognized as an important factor affecting the functions of terrestrial ecosystems and climate change (Pickett et al., 2001; Goldewijk & Ramnakutty, 2004; Zhou et al., 2004; Foley et al., 2005; Kaufmann et al., 2007). Hence, timely mapping human settlement, especially at regional and global scales, has considerable significance and has already attracted attention in the past decade (Elvidge et al., 1997a, 2001; Sudhira et al., 2004; Ridd & Hipple, 2006).

The urban landscape is a complexity consisting of different land covers, such as trees, lawns, impervious surfaces, and water. In remotely sensed data, especially in coarse spatial resolution images, many different land covers may be mixed in a pixel. This problem often induces difficulty in extracting settlements from remotely sensed data. Previous research for mapping human settlements is often based on high or medium spatial resolution images (e.g., IKONOS, Landsat TM/ETM+) for individual cities (Lu & Weng, 2006; Ridd & Hipple, 2006). Although many techniques, such as different per-pixel based classification approaches and spectral mixture analysis, have been used for mapping settlements or impervious

* Corresponding author. Tel.: +1 334 844 1062; fax: +1 334 844 1084.
E-mail address: LUDS@auburn.edu (D. Lu).

0034-4257/$ – see front matter © 2008 Elsevier Inc. All rights reserved.
doi:10.1016/j.rse.2008.05.009

surface areas from medium spatial resolution images (Wu & Murray, 2003; Yang et al., 2003; Lu & Weng, 2006; Powell et al., 2007), they are not suitable for regional or global settlement estimation because of the mixed pixel problems and complex landscape. However, mapping human settlements at regional and global scales has become an urgent task because of the increasing pressures from rapid urbanization and associated environmental problems. If high or medium spatial resolution images are used at the regional or global scale, the cost for image purchase, and the time and labor required for processing and interpreting these images could become prohibitive. The frequent cloud conditions in a large area also make it difficult to collect a large number of good-quality images within the same year. It is imperative to develop new approaches to timely and accurately map settlements in a large area with coarse spatial resolution images; however, no suitable approaches are available for mapping settlements at regional and global scales. Hence, this research aims to develop a new approach to map human settlements at the regional scale with the integration of coarse and medium spatial resolution images.

In this research, southeastern China was selected as the study area because of its rapid urbanization since the early 1980s. Landsat ETM+ (Enhanced Thematic Mapper Plus) images were used to map settlements in the selected sites at the local scale. Defense Meteorological Satellite Program's (DMSP) Operational Line-scan System (OLS) (hereafter, DMSP-OLS) and Terra Moderate Resolution Imaging Spectroradiometer (MODIS) were used to map pixel-based settlement images. A regression model, which was established with the combination of ETM+ derived settlements, DMSP-OLS, and MODIS NDVI (Normalized Difference Vegetation Index) data, was used to estimate fractional settlements for the entire study area.

2. Background

The DMSP-OLS uses two instruments (i.e., visible-near infrared and thermal infrared telescopes) to provide both daytime and nighttime images of the Earth (Elvidge et al., 1997b). The visible-near infrared telescope is sensitive to radiation from 0.40–1.10 μm, and the thermal infrared telescope is sensitive to radiation from 10.0–13.4 μm and 190 to 310 K. A telescope pixel is 0.55 km at fine mode and 2.7 km at smooth mode. Low resolution values are the mean of pixel values at a window size of 5 by 5 at fine mode (http://www.ngdc.noaa.gov/dmsp/sensors/ols.html). Time-series analysis of collected images within a calendar year is used to distinguish stable lights produced by cities and towns from ephemeral lights arising from fires and lightings, and to remove clouds. The time-series data sets are then composed to generate a city-light image with spatial resolution of 1 km. Much previous literature has described the characteristics of the DMSP-OLS data (e.g., Imhoff et al., 1997a,b; Elvidge et al., 1997a,b,c, 1999). The DMSP-OLS nighttime image (city lights or stable lights) reflects the existence of human activities. The intensity of the city's nighttime lighting is closely related to population density and economic conditions (Elvidge et al., 2007). Therefore, the DMSP-OLS data are often used to map urban areas or human settlements (Elvidge et al., 1997b; Imhoff et al., 1997a,b; Milesi et al., 2003a; Gallo et al., 2004) and to estimate demographic and socioeconomic variables (Welch, 1980; Sutton et al., 1997; Lo, 2001, 2002 Sutton et al., 2001; Sutton, 2003; Amaral et al., 2005, 2006). More applications of DMSP-OLS data were summarized by Elvidge et al. (2007).

Two kinds of data formats in the DMSP-OLS images are often used. One is the percent occurrence, or the percentage of time during a grid cell which was lit in the building of the composite (Imhoff et al., 1997b); and the other is the digital number ranging from 0 to 63 (Elvidge et al., 1999). A common application of the DMSP-OLS data is to map urban areas or human settlements with the thresholding technique (Imhoff et al., 1997a,b; Lawrence et al., 2002). A challenge of this technique is to determine appropriate thresholds. No general rules are available for guiding the selection of threshold values. In previous research, when the pixel values of DMSP-OLS stable-light image ranged from 0 to 100%, Imhoff et al. (1997a) used a threshold of 89% to detect urban areas in the continental U.S.; and Amaral et al. (2005) used a threshold of 30% to extract a binary image with the nighttime light area and background in the Brazilian Amazonia. When the pixel values of DMSP-OLS image appeared as digital numbers (DN) ranging from 0 to 63, a threshold of 50 was regarded as optimal in southeastern U.S. (Milesi et al., 2003b). In reality a single threshold could significantly overestimate urban areas, but could omit a large number of towns and villages with a relatively small proportion of settlements. The significant differences of energy availability and consumption, levels of economic development, and density of settlements in a regional or global scale may result in significantly different pixel values in the DMSP-OLS imagery (Small et al., 2005). Thus, the urban distribution derived from a single threshold technique may produce a large error in the spatial pattern. Some previous research has recognized this problem and has used multiple thresholds to map settlements at three levels, for instance, urban (>94%), peri-urban (8–94%), and unpopulated places (<8%) in Egypt (Lawrence et al., 2002), or urban (>89%), suburban (25–88%), and rural (<24%) in U.S. Historical Climatology Network (Owen et al., 1998). Depending on the levels of economic development, Henderson et al. (2003) identified the optimal threshold of 92% for San Francisco, USA, 97% for Beijing, China, and 88% for Lhasa, China. Sutton et al. (2001) used three thresholds of 40%, 80%, and 90% for mapping urban areas based on the level of gross domestic product (GDP) per capita in the world.

Although previous research with the threshold-based approach has advanced the understanding of settlement mapping from DMSP-OLS data, there remain some problems with the threshold-based approach. First, selecting an appropriate threshold is difficult and seems subjective. No single threshold is appropriate in a large area because of the different levels of socioeconomic development. Secondly, a large uncertainty may be generated by the mixed pixel problem and the impacts of background such as ephemeral light, low-level illumination, and glint of light into adjacent water bodies. Finally, a large number of small settlements may be lost, and the spatial pattern information is reduced significantly. Elvidge et al. (2007) summarized eleven specific shortcomings of the DMSP-OLS data. Fig. 1 clearly illustrates some important problems (see the Methods section for the data collection) by examining the images among DMSP-OLS, Terra MODIS color composite, and Landsat ETM+ color composite (assigned near infrared, shortwave infrared, and visible bands as red, green and blue). For instance, rivers, lakes, and forests within or nearby Hangzhou, China had similar high DN values to the settlements in the DMSP-OLS image. However, water bodies and forests had significantly different spectral features with settlements in MODIS and ETM+ color composites. On the other hand, medium- and low-intensity residential areas had DN values of less than 50, thus, they would be lost when a threshold approach was used, resulting in significant underestimation of settlements. Obviously, the threshold-based technique cannot accurately map the spatial pattern of settlements.

3. Methods

3.1. Study area

Southeastern China has experienced rapid urbanization since the early 1980s. The selected study area covered 10 provinces and two metropolises — Shanghai and Hong Kong (Fig. 2). The study area accounted for 15.7% of the total area in China, but the population and gross domestic product (GDP) accounted for 44.2% and 54.3% according to the China Statistical Yearbook in 2006 (Bureau of Statistics of China, 2006a) [Note: these percentages did not include Hong Kong with a population of 6.91 million and GDP of $253.1 billion in 2006 according to Wikipedia record (http://en.wikipedia.org/wiki/

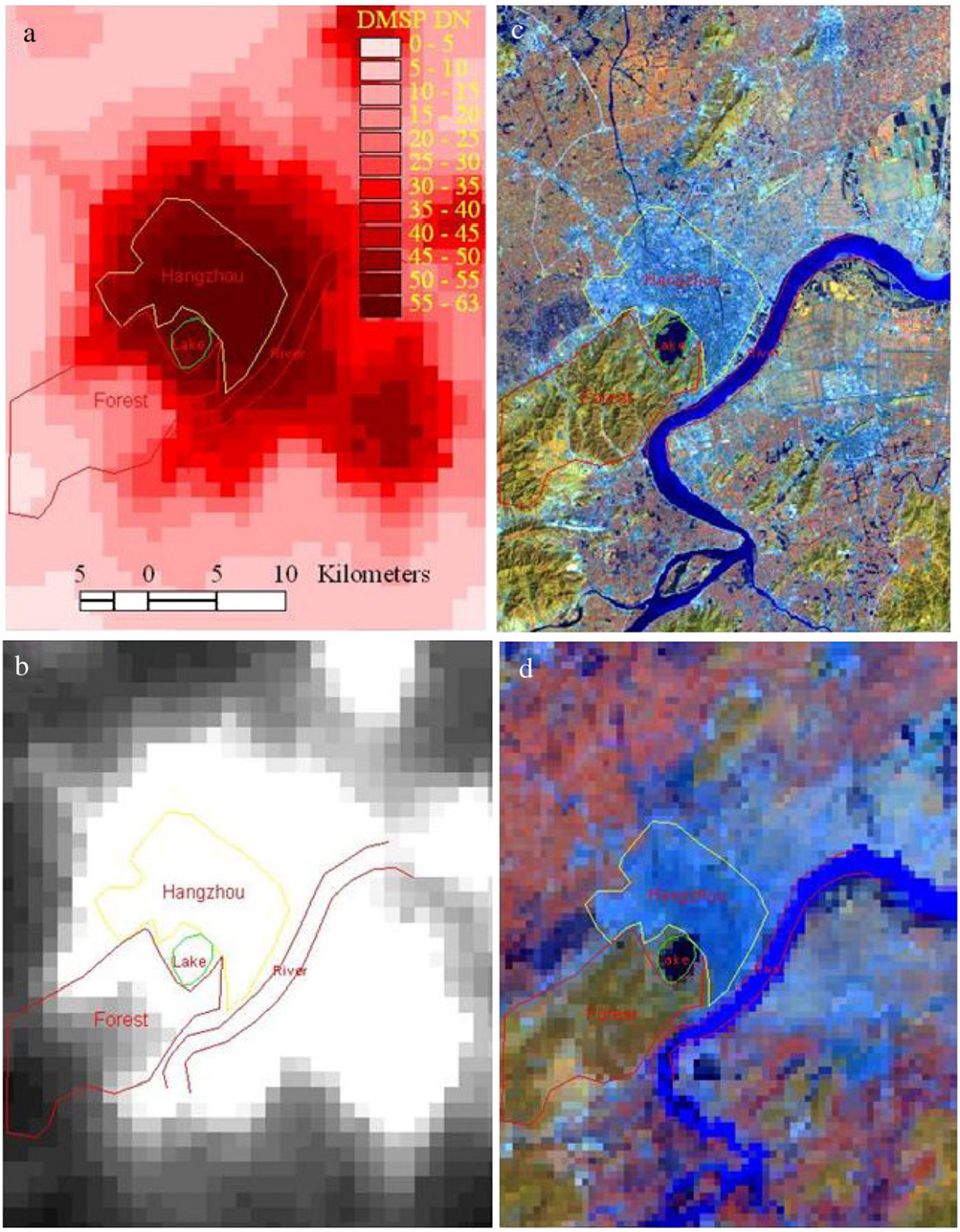

Fig. 1. A comparison of human settlements appeared in DMSP-OLS, MODIS, and Landsat ETM+ images (Note: a — DMSP-OLS false color image based on sliced DN values; b — DMSP-OLS DN with black and white image; c — Landsat ETM+ color composite; and d — MODIS color composite (assigning near infrared, shortwave infrared, and visible bands as red, green and blue).

Hong_Kong)]. There are three megacities with more than five million inhabitants, 23 megacities (this number accounts for 45.1% in China) with a population ranging from 1 to 5 million, and 35 cities (accounting for 37.2%) with a population between 0.5 to 1 million in this study area, according to China City Statistical Yearbook in 2006 (Bureau of Statistics of China, 2006b).

3.2. Data collection and preprocessing

DMSP-OLS stable light, Terra MODIS surface reflectance, multi-temporal MODIS NDVI, and Landsat ETM+ images were used in this research and their major characteristics were summarized in Table 1. All the selected data sets were acquired in 2000. The DMSP-OLS nighttime-lights data with 1 km spatial resolution were downloaded from the National Geophysical Data Center (NGDC) [http://www.ngdc.noaa.gov/dmsp/global_composites_v2.html (last access on August 7, 2007)]. The DMSP-OLS image has DN values ranged from 0 to 63. The selected DMSP-OLS image was a composite based on time-series archived DMSP-OLS images in the calendar year of 2000. A detailed description of DMSP-OLS data is found in Elvidge et al. (1997b, 1999). The stable light data with geographic (Lat/Lon) projection were reprojected to Albers Conical Equal Area projection and the nearest neighbor resampling algorithm was used during the reprojection procedure.

Terra MODIS surface reflectance (MOD09A1) and NDVI (MOD13A2) images were downloaded from the USGS (United State Geographic

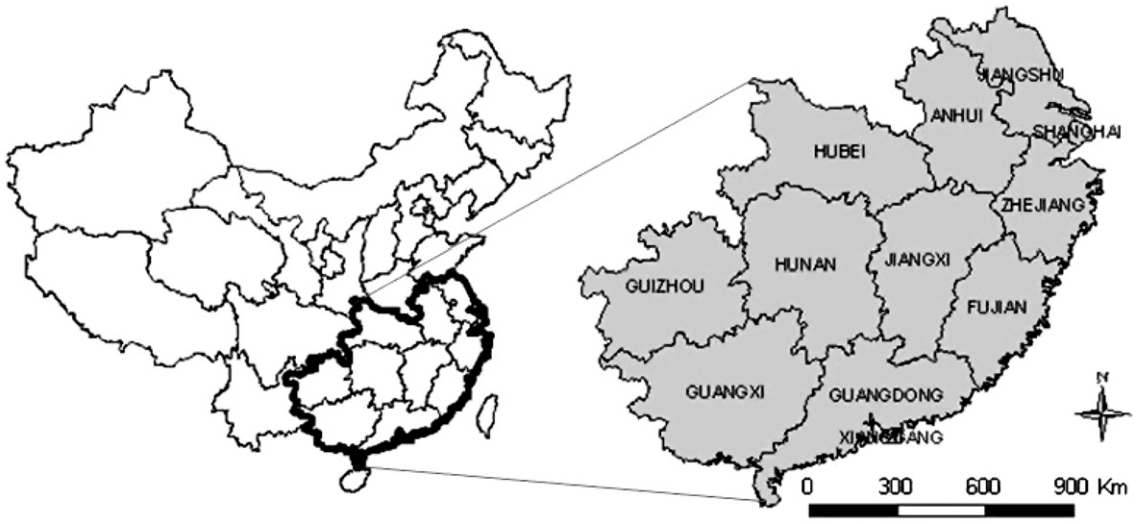

Fig. 2. Study area —southeastern China covering 10 provinces, Shanghai, and Hong Kong by overlaying a boundary layer at provincial level.

Survey) (Global Visualization Viewer). Previous literature has detailed the description of developing MOD09A1 and MOD13A2 products (e.g., Justice et al., 2002). The MODIS data (including surface reflectance and multitemporal NDVI images) with sinusoidal projection were reprojected to Albers Conical Equal Area projection. A bilinear interpolation algorithm was used to resample MODIS surface reflectance images with their original spatial resolution of 463 m into a pixel size of 1 km by 1 km, and the nearest neighbor resampling algorithm was used to resample multitemporal MODIS NDVI images for keeping the pixel size of 1 km by 1 km during the reprojection procedure.

Six scenes of Landsat ETM+ images were selected within the study area. The ETM+ six reflective bands (e.g., visible, near infrared, and shortwave infrared) with 28.5 m spatial resolution were used in this research (the thermal band and the panchromatic band were not used). All selected ETM+ images with the Universal Transverse Mercator (UTM) coordinate system were reprojected to Albers Conical Equal Area projection. The nearest neighbor algorithm was used to resample the ETM+ images into a pixel size of 25 m by 25 m.

The strategy for mapping human settlements at the regional scale based on a combination of medium and coarse spatial resolution images is illustrated in Fig. 3. The ETM+ images were used to map settlements at the local scale with a hybrid approach. A combination of MODIS and DMSP-OLS data was used to mask out the pixels with non-settlement land covers. Regression models were then established to calibrate the settlement results at the regional scale.

Table 1
Remotely sensed data used in research

Sensor	Resolution	Acquisition date
DMSP-OLS	The annual image product with the grid cell size of 1 km by 1 km was developed from the time-series DMSP-OLS images with nominal spatial resolution of 0.55 km. The selected DMSP-OLS image has DN values ranging from 0 to 63.	A cloud-free composite developed from all available archived DMSP-OLS data for the calendar year of 2000.
MODIS	Spatial resolution of 500 m for MODIS surface reflectance image (MOD09A1). Band 5 was not used due to the strip problem. Spatial resolution of 1 km for multitemporal MODIS NDVI images (MOD13A2).	8-day composite, acquired in Sept 13–20, 2000 (MODIS mosaic image based on images of h27v05, h27v06, h28v05, and h28v06 scenes). 16-day composite; multitemporal NDVI mosaic images were collected between April and October 2000.
Landsat ETM+	Six reflective bands with 28.5 m spatial resolution (thermal and panchromatic bands were not used in this research).	Path/row: Acquisition date 119/39: Oct 11, 2000 120/37: Sep 16, 2000 122/41: Sep 14, 2000 122/44: Sep 14, 2000 124/45: Oct 30, 2000 122/37: Sep 14, 2000

3.3. Settlement mapping from Landsat ETM+ images

Accurate settlement mapping from the selected ETM+ images is a prerequisite because this data set is used as a reference for establishing regression models and for accuracy assessment. In reality, settlement is a complex combination of different impervious surface materials. Previous research has indicated the difficulty in separating settlements from other land covers based on spectral signatures with traditional per-pixel based classification approaches (Lu & Weng, 2004; 2005). One possible approach is to incorporate land surface temperature to separate dark-color impervious surfaces from water based on their differences in land surface temperature (Lu & Weng, 2006). However, the relatively coarse spatial resolution in thermal images (e.g., 120 m in TM thermal band vs. 28.5 m in TM multispectral bands) often resulted in overestimation of impervious surfaces (Lu & Weng, 2006). Therefore, in this research, we developed a hybrid approach, which consisted of matched filtering (partial unmixing), expert rules, stratification, and unsupervised classification, to map settlements from the ETM+ images.

The matched filtering approach is used to find the abundance of a user-defined endmember with the partial unmixing technique, which maximizes the response of the selected endmember and suppresses the response of the background (Boardman et al., 1995). This approach provides a rapid way to detect the specific material based on the matches to the selected endmember spectra. The resultant image from matched filtering appears as a gray-scale image representing the relative degree of match to the selected spectra. A detailed description of the match filtering approach is provided in Boardman et al. (1995). In this research, settlement endmembers was selected on the ETM+ image through visual interpretation of the ETM+ color composites. Because of the complexity of settlement materials, it is difficult to identify one settlement to represent all settlements in the study area. Thus, three types of settlements, i.e., settlements with high-, medium-, and low-spectral signatures, were selected. Matched filtering was then used to unmix the ETM+ six reflective bands into fraction images based on the selected settlement endmembers. A comparative visual analysis of the three fraction images indicated that the settlement endmember having medium spectral features provided the best results; and thus,

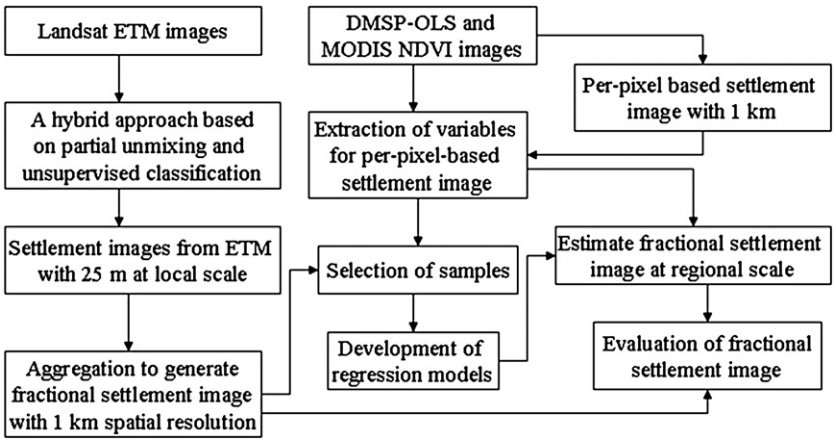

Fig. 3. Framework of developing fractional settlements at regional scale with the combination of medium and coarse spatial resolution images.

this fraction image was further examined. Analysis of samples of settlements showed that a threshold of 0.1 was optimal to extract the settlement information from the selected fraction image. Thus, a binary image for the initial settlements was produced based on the rule: if a pixel value in the fraction image was greater than 0.1, assigned 1 (settlements) to this pixel, otherwise, assigned 0 (non-settlements) to the pixel.

The confusion of some bright-color settlements with bare soils and dark-color settlements with water made the initial settlements overestimated. Therefore, removing non-settlement pixels in the initial settlement image was required. In this research, the spectral signatures of the initial settlement image were extracted from the ETM+ reflective bands with an expert rule, i.e., if the pixel value was 1 in the initial settlement image, extracted the spectral signatures from the ETM+ six reflective bands, otherwise, assigned 0 to the pixel. The ISODATA unsupervised classification approach was used to classify the extracted spectral signatures into 60 clusters. The cluster image was then overlaid on the ETM+ color composite. The analyst was responsible to examine each cluster and to assign each cluster as a settlement or other land cover. The final settlement image was again overlaid on the ETM+ color composite to visually examine the success, or not, in mapping the settlements while removing all non-settlements in the image. This procedure for settlement mapping was applied to all selected ETM+ images. The final settlement image was a binary format with 1 representing the settlement and 0 representing other land covers. Finally, the settlement image with 25 m spatial resolution was aggregated to generate proportional settlement values in a new data set with a pixel size of 1 km by 1 km to match the same spatial resolution with MODIS and DMSP-OLS data.

3.4. Spectral analysis of settlements from DMSP-OLS data

A total of 800 sample plots with a window size of 1 km by 1 km for each plot were randomly selected from the fractional settlement images which were developed from the ETM+ images. The sample plots were linked to the DMSP-OLS image to extract the DN values for examining the relationship between fractional settlements and DMSP-OLS DN values. The fractional settlement values ranging from 0 to 1.0 were separated into 10 groups with an interval of 0.1. The boxplot approach was used to examine DMSP-OLS DN features, representing graphically the distribution of fractional settlements in a pixel against the DMSP-OLS DN value. Fig. 4 shows the complexity of the relationship between fractions of settlements and DMSP-OLS DN values and indicates the problem using the threshold-based technique in mapping settlements or urban areas because low DN values in the DMSP-OLS image (1 km spatial resolution) could contain a certain proportion of settlements in a pixel, as shown in Landsat images (25 m spatial resolution here) (see Fig. 1). The DN values in the DMSP-OLS image may range from 3 to 63, depending on the proportion of settlements in a pixel. The majority of pixels with fraction values of greater than 0.9 had DN values of greater than 50. Some pixels with fraction values ranging from 0.6 and 0.9 had also DN values of greater than 50, but most of them had DN values between 15 and 50. If the fraction values were in 0.1–0.5, the DN values ranged from 3 to 30. This implied that similar DN values could contain a significantly different proportion of settlements in a pixel. This problem could result in a large uncertainty in settlement estimation and loss of spatial information based on DMSP-OLS data at the regional scale.

3.5. Pixel-based settlement extraction from Terra MODIS and DMSP-OLS images

Previous research has indicated that the vegetation index, or vegetation abundance, is closely correlated in a negative manner with

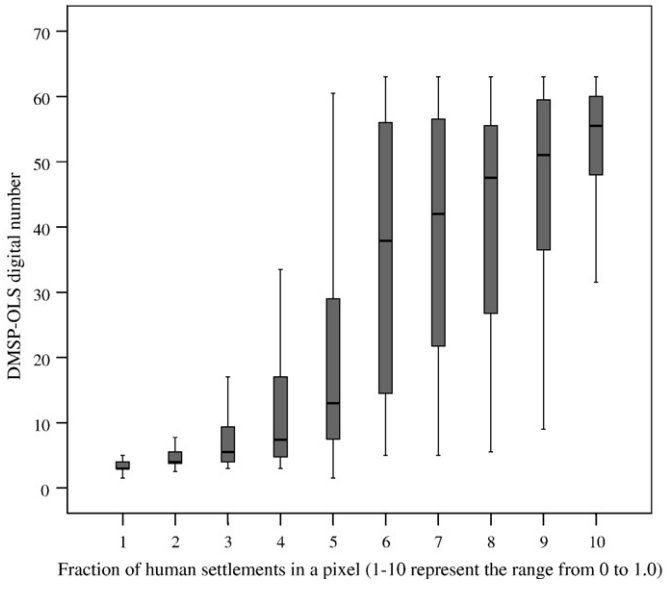

Fig. 4. Relationship between DMSP-OLS DN and fractional settlements in a grid cell of 1 km (note: the fraction value of settlements in a pixel was derived from Landsat ETM+ images. This graph was based on the 800 samples which were randomly selected from the settlement images developed from Landsat ETM+ images and the corresponding DMSP-OLS DN image).

Table 2
Regression models developed from the combination of coarse and medium spatial resolution images

Regression method	Variables used	Best regression model ($Y=a+bx_1+cx_2$)	R^2	F test	t test		
					a	b	c
Linear and nonlinear regression analysis	DMSP	FSM = −0.059 + 0.207Ln(DMSP)	0.645	916.4	−2.8*	30.3	
	$NDVI_{max}$	FSM = 1.267–1.321 $NDVI_{max}$	0.587	716.0	44.4	−26.8	
	Settlement index	FSM = 0.657 + 0.241Ln(index)	0.664	995.5	79.8	31.6	
Stepwise regression analysis	DMSP, Ln(DMSP), $DMSP_{nor}$, $NDVI_{max}$, index	FSM = 0.469 + 0.136Ln(DMSP) − 0.588$NDVI_{max}$	0.686	550.4	6.9	12.6	−8.1

*0.005 level. Others at less than 0.0001.
Note: FSM represents fractional settlements; R^2 represents coefficient of determination for evaluation of the regression model performance.

impervious surfaces (Weng et al., 2004) and has been used for the estimation of impervious surfaces (Gillies et al., 2003; Bauer et al., 2004). However, bare soils are often a problem when using a single-date vegetation index image. For example, in agricultural lands, different seasons could have different surface covers such as grass, crop, and bare soil. In order to better separate impervious surfaces, or settlements, from bare soils, use of multitemporal NDVI can effectively reduce the impact of bare soils. In a large area, an important role of using multitemporal NDVI images is to remove the impact of cloud contamination. Therefore, multitemporal NDVI images were used in this research to generate a new NDVI composite (i.e., $NDVI_{max}$) with the maximum algorithm as expressed in Eq. (1).

$$NDVI_{max} = MAX[NDVI_1, NDVI_2, \ldots, NDVI_n], \quad (1)$$

where $NDVI_1$, $NDVI_2$, …, $NDVI_n$ are the multitemporal MODIS NDVI images acquired during April and October in 2000.

Comparing the settlements from ETM+ images with corresponding MODIS NDVI and DMSP-OLS data indicated that high fractional settlements in a pixel had generally high DN values in the DMSP-OLS image and had low values in the NDVI image. Different remotely sensed data have their own characteristics and combined use of them could provide more information than their individuals. Data fusion is the most common approach to integrate multiple sensor data sources (Lu & Weng, 2007), and the common data sources include SPOT, Landsat, and radar (Yocky, 1996; Haack et al., 2002; Ban, 2003). However, rarely has research examined the data fusion approaches for multiple sensors of coarse spatial resolution images.

The 6-bit DMSP-OLS data (DN ranges within 0 and 63) often resulted in data saturation in urban landscape (Elvidge et al., 2007) and difficulty in separating different land covers. As shown in Fig. 4, if no city lights exist in a land cover such as forest lands, bare soils, and water bodies, the DMSP-OLS DN values are close to zero. However, because of the different levels of economic development, energy availability and consumption, the similar DN values in the DMSP-OLS image could have a significantly different proportion of settlements in a pixel. Therefore, the traditional thresholding technique cannot be accurately used to map human settlements from DMSP-OLS data, but the DMSP-OLS data can be used first to mask out the non-settlement land covers such as forest, agricultural lands, and water.

The 16-bit MODIS data (0–65,535) provided more detail information for separating different land covers, but MODIS data cannot be directly used for mapping human settlements because of the complexity of settlement materials and the mixture of settlements and other land covers in spectral signatures. In urban landscapes, vegetation distribution is closely related to the patterns of settlements (Weng et al., 2004), thus, the vegetation index can be used to estimate human settlements (Bauer et al., 2004). However, non-vegetation land covers, such as bare soils, water, and human settlements have similar values in the NDVI image; thus, NDVI images are not suitable for directly separating human settlements from water and bare soils. Because of the complexity of human settlements and the mixed pixel problem in the coarse spatial resolution image, the pixel-based classification approach cannot accurately map human settlements based on the MODIS NDVI images.

In theory, NDVI image have values ranging from −1 to +1. Because of the coarse spatial resolution in MODIS NDVI, the land surface covers, except large water bodies, have data ranges between 0 and 1 in the $NDVI_{max}$ image during the growing season. In order to match the data range between $NDVI_{max}$ and DMSP-OLS data sets, it is necessary to convert the DMSP-OLS DN values into a floating format with Eq. (2) so that the data values can be in the range of 0 and 1.

$$OLS_{nor} = \frac{OLS - OLS_{min}}{OLS_{max} - OLS_{min}}, \quad (2)$$

where OLS_{nor} is the normalized value of the DMSP-OLS DN image. OLS_{min} and OLS_{max} are the minimum and maximum values in the DMSP-OLS image, i.e., 0 and 63 here.

Because of different characteristics between DMSP-OLS and MODIS $NDVI_{max}$ data sets in separating settlements from other land covers as discussed above, a combined use of both data sets could provide new insights for mapping settlements at regional or global scale. Therefore, we developed an index called human settlement index in this paper, as expressed in Eq. (3).

$$Human\_settlement\_Index = \frac{(1 - NDVI_{max}) + OLS_{nor}}{(1 - OLS_{nor}) + NDVI_{max} + OLS_{nor} * NDVI_{max}} \quad (3)$$

In general, higher proportion of settlements in a pixel should result in a lower value in MODIS $NDVI_{max}$ and a higher value in DMSP-OLS, thus generating higher value in this index. As different levels of economic development and energy consumption affect the city lights, as shown in Fig. 4, similar DMSP-OLS DN values could have significantly different proportion of settlements in various regions. However, in urban landscape, vegetation abundance is highly correlated with impervious surface (Weng et al., 2004). Therefore, incorporation of vegetation information into the city light data set can reduce the effects of external factors such as economic development levels on the DMSP-OLS DN values.

Sample plots with a window size of 1 km^2 were selected based on the ETM+ derived settlement images, and these plots were linked to the settlement index image to extract the value for each sample. A threshold was then identified, based on a comparative analysis of the

Table 3
Comparison of accuracy assessments among the selected models based on randomly sampled 233 samples at pixel level

Methods	R	RMSE
DMSP-OLS	0.81	0.162
$NDVI_{max}$	0.72	0.194
Settlement index	0.82	0.158
Both DMSP-OLS and $NDVI_{max}$	0.83	0.156

Note: R represents correlation coefficient between estimate and reference data. RMSE represents root-mean square error.

samples of settlements and non-settlements, and used to extract the initial pixel-based settlement image. The initial settlement image may contain some non-settlement pixels because of the complexity of urban landscapes and the confusion of settlements, bare soils, and water bodies on the $NDVI_{max}$ and DMSP-OLS images. A similar approach as used in ETM+ images for removing non-settlement pixels was also used for MODIS data, that is, the initial settlement image was a binary image with 1 representing settlement and 0 representing other land covers. When the pixel value was 1 in the initial settlement image, the value of MODIS surface reflectance was extracted, otherwise, 0 was assigned to this pixel. The extracted MODIS surface reflectance image for the initial settlements was then classified into 80 clusters using the ISODATA approach. The analyst finally refined the initial settlement image by removing the clusters of non-settlements based on visually interpreting the clusters on the MODIS color composite by assistance of ETM+ color composites.

3.6. Fractional settlement estimation with regression models

Mixed pixels have been recognized as a major problem affecting the effective use of remotely sensed data in urban land-use/cover classification (Fisher, 1997; Cracknell, 1998). It is especially true when coarse spatial resolution images such as MODIS and DMSP-OLS are used for settlement mapping because of the complex urban landscapes. It is important to exclude the non-settlement fraction in a pixel in order to accurately reflect the settlement areas and their spatial patterns. Here we developed regression models for estimating fractional settlements. The ETM+ derived fractional settlement data set was used as a dependent variable. DMSP-OLS, normalized DMSP-OLS, logarithmic DMSP-OLS, $NDVI_{max}$, and human settlement index were used as a single independent variable in linear and nonlinear regression analysis, or as multiple variables in the stepwise regression analysis. The coefficient of determination (R^2) was used to evaluate the regression model performance because it measured the percentage of variation explained by the regression model. *F* test was used to examine whether the regression model was significant or not, and *t* test was used to examine whether the constant and beta values were significant or not. The regression model whose *F* and *t* tests were significant and whose R^2 value was the highest was finally selected for further analysis. The selected regression models were then used to estimate the fractional settlements for the entire study area. In order to develop regression models, a total of 800 sample plots with a pixel size of 1 km^2 were randomly selected based on the fractional settlements from six ETM+ images. Approximately 70% of these

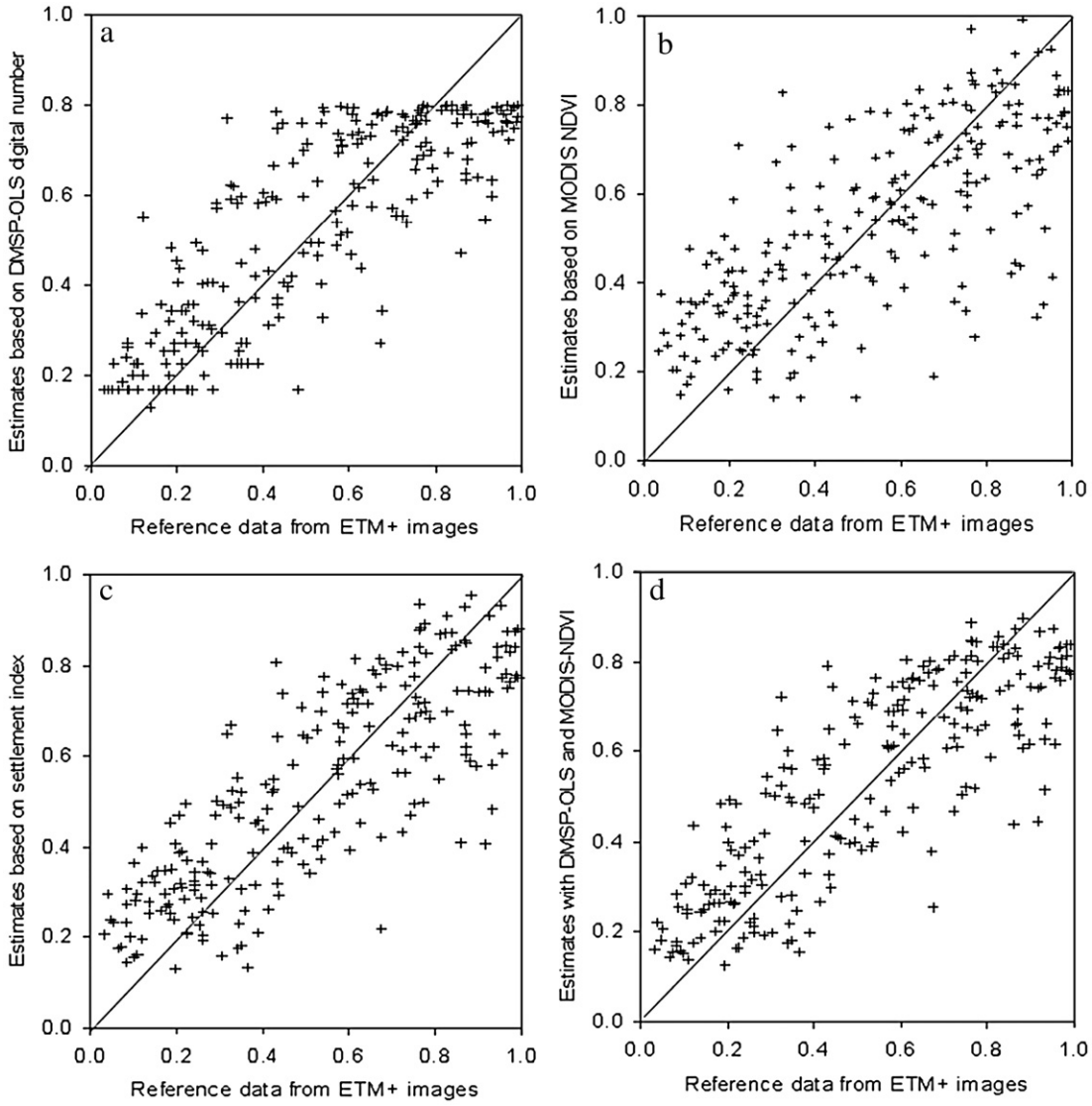

Fig. 5. A comparison of scatterplots based on estimates and reference data (note: the reference data were from ETM+ images and the estimates were from the selected regression models based on 233 samples at 1 pixel level; Regression models based on DMSP-OLS (a), $NDVI_{max}$ (b), human settlement index (c), and both DMSP-OLS and $NDVI_{max}$(d)).

samples were randomly resampled for developing the regression models and the rest for accuracy assessment.

3.7. Evaluation of fractional settlement estimates

Accuracy assessment is an important part in evaluating the modeling results. In this research, the root-mean square error (RMSE) was used. Of the 800 samples, approximately 30% of the samples were randomly selected for model assessment. Correlation coefficients between estimates and the reference data, and their scatterplots were used to examine the quality of model performance. In addition, a comparative analysis of the spatial patterns of the estimated settlements from each selected regression model was conducted to identify the suitable regression model for mapping the spatial distribution of the fractional human settlements.

4. Results

4.1. Settlement mapping from Landsat ETM+ images

Settlements at selected sites were developed from ETM+ images and used as reference data. Although no quantitative accuracy assessment was conducted for the ETM+ derived settlement images, a visual examination by overlaying the settlement images on

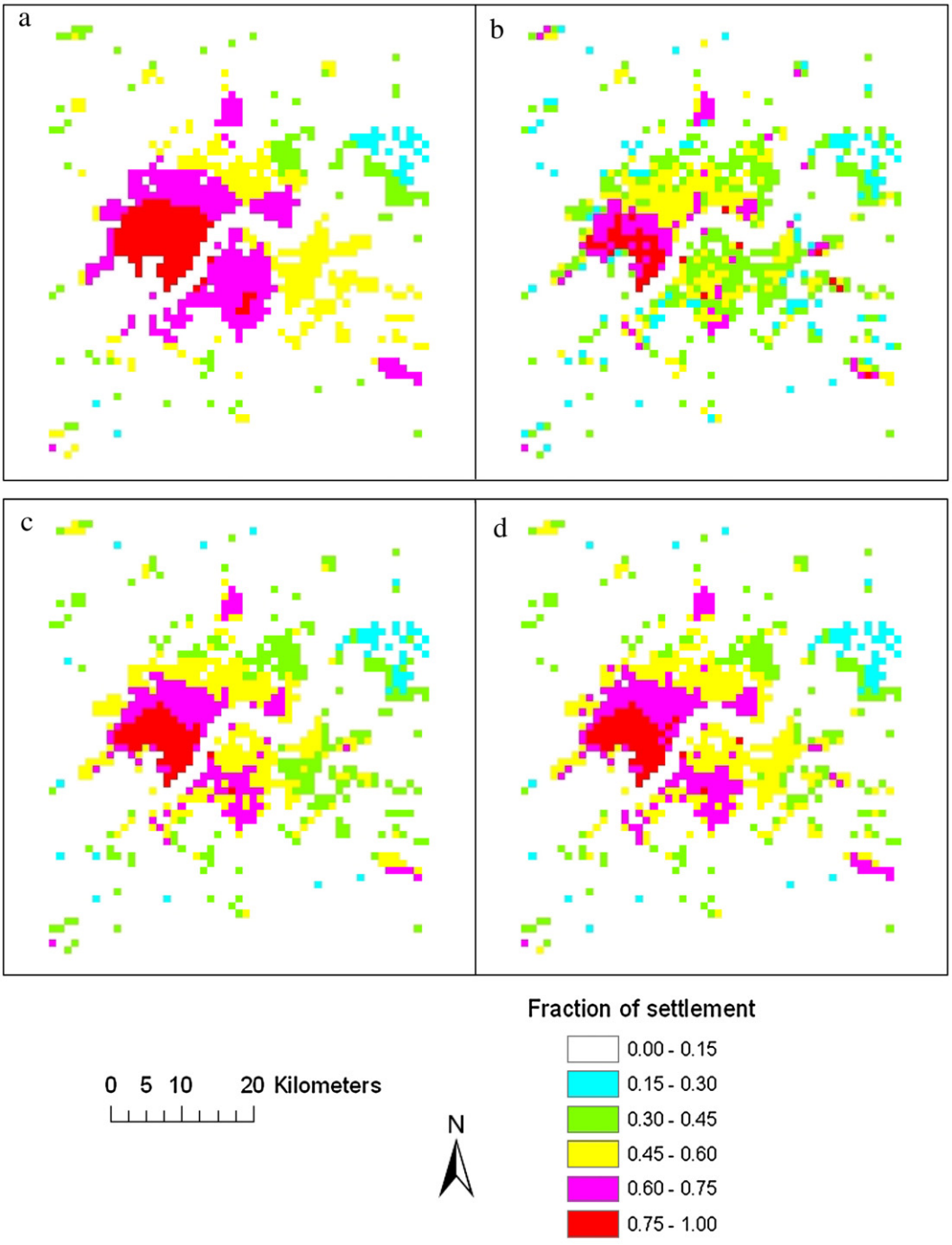

Fig. 6. A comparison of spatial patterns of the human settlement estimates among the selected regression models (Note: Regression models based on DMSP-OLS (a), $NDVI_{max}$ (b), human settlement index (c), and both DMSP-OLS and $NDVI_{max}$(d)).

corresponding ETM+ color composites was conducted. The qualitative evaluation showed the success using the hybrid approach for mapping settlements at selected sites. The fractional settlement values were highest in urban areas, and then they were decreased gradually in suburban and rural areas. Because of the complexity of the urban landscape, settlement areas could be overestimated in the low-intensity residential areas based on the pixel-based classification approach (Lu & Weng, 2006). In this research, unsupervised classification provided an alternative to separate low-intensity residential areas from forests because the analyst can make use of his/her knowledge about the study area and different spatial patterns between forests and low-intensity residential areas. The hybrid approach used in this paper has further improved the settlement extraction performance based on previous research (Lu & Weng, 2006).

4.2. Evaluation of model estimates

A comparative analysis of the selected four regression models (Table 2) indicated that all selected regression models were significant based on *F* test at less than 0.0001. The constant and beta values for each regression model were also significant based on *t* test at less than 0.0001, except the constant in the single DMSP-OLS based regression model (significant at 0.005). Overall, the regression models, by using both DMSP-OLS and $NDVI_{max}$, either integrated as a settlement index or as a combination of both variables, provided relatively higher R^2

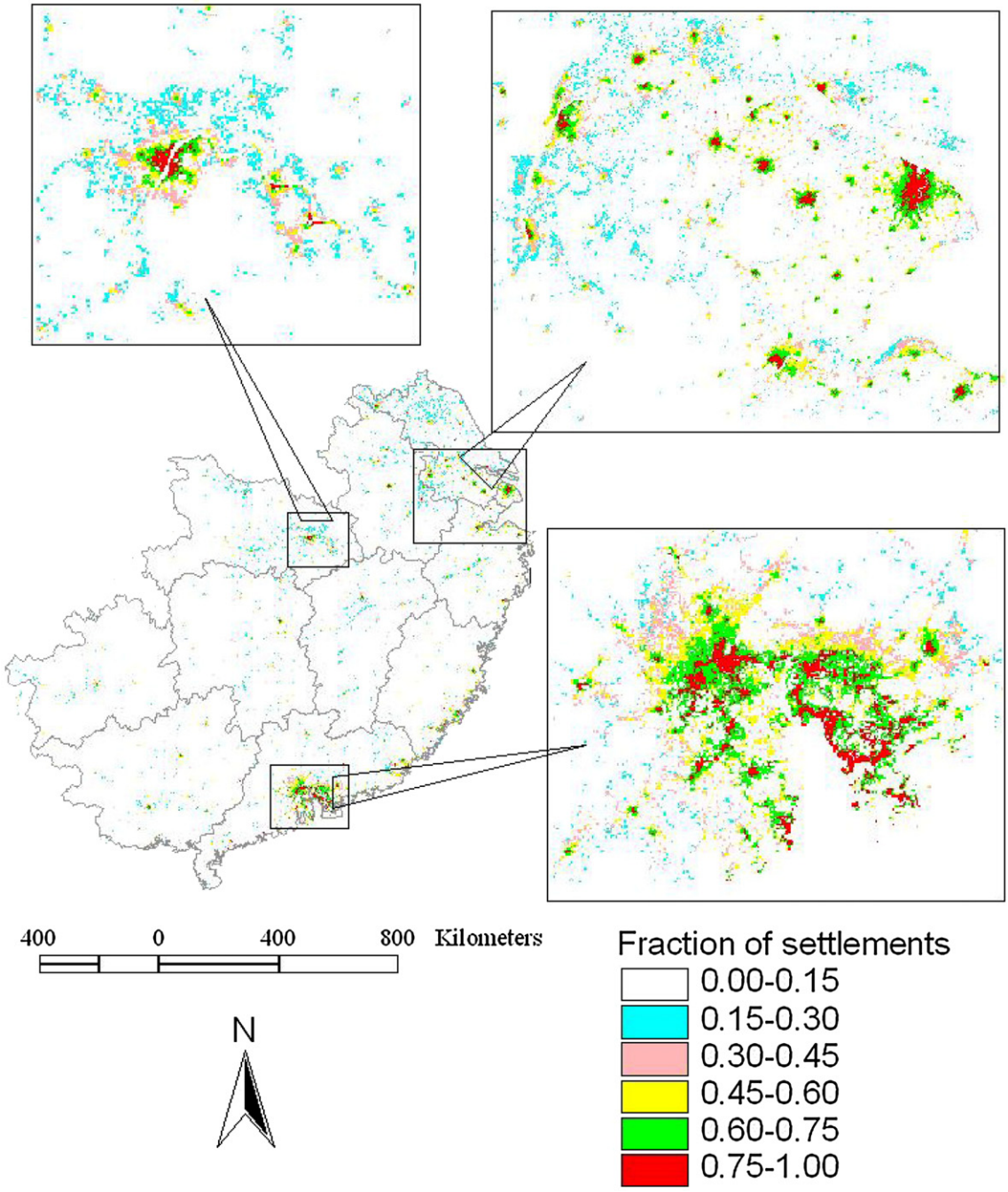

Fig. 7. Fractional settlements developed from a combination of DMSP-OLS, MODIS $NDVI_{max}$, and Landsat ETM+ images in 2000 in southeastern China, highlighting three urban regions (the administrative boundary at the provincial level was overlaid on the human settlement image).

values than by using single $NDVI_{max}$ or DMSP-OLS variable. This implied that integration of both sensor data could generate a better estimation performance than a single sensor data set. Except the regression model based on a single $NDVI_{max}$ variable, the other three regression models had similar performance and similar RMSE values, as shown in Table 3. However, if we carefully examined the scatterplots between the estimates and reference data (Fig. 5), we can find their differences. For instance, the single DMSP-OLS based regression model has the data saturation problem that it cannot accurately estimate the fraction values when the fraction of settlements in a pixel is greater than 0.8 (Fig. 5a). The single $NDVI_{max}$ based regression model has a large variation, implying that this method may produce a larger error for individual pixels than other selected models (Fig. 5b). A comparison of Fig. 5c and d showed a similar performance, but when the pixel had high proportion of settlements such as greater than 0.8, the regression model based on human settlement index appeared better estimation performance than that based on both DMSP-OLS and $NDVI_{max}$ variables. All selected regression models have the trend that overestimate the fraction values for those pixels with a relative small fraction of settlements, such as less than 0.2. Overall, Fig. 5 indicates that the regression model based on the human settlement index may provide the best estimation results.

Fig. 6 provides an example showing the different spatial patterns of fractional settlement images from the selected four regression models. The DMSP-OLS based model overestimated the number of pixels with relatively high fraction values, such as greater than 0.45 (see Fig. 6a), except the pixels with high fraction settlements due to the data saturation problem as shown in Fig. 5a. In contrast, the $NDVI_{max}$ based model underestimated the pixels with relatively high fractional settlements, such as greater than 0.6 (Fig. 6b). The regression models based on the human settlement index, or combined DMSP-OLS and $NDVI_{max}$ variables provided similar spatial patterns, implying that both regression models had similar estimation performance. Fig. 7 provides an example which was estimated using the regression model based on both DMSP-OLS and $NDVI_{max}$ variables, showing the fractional settlement image highlighting three megacities and their surrounding areas in south, east, and central China. It indicated that the core urban areas had higher fraction values than suburban and rural areas, and the sites with small fractional settlements were successfully mapped. As Fig. 8a indicated that no matter one single threshold or multiple thresholds were used, the threshold technique cannot accurately map the spatial patterns of different proportional settlements. This research also showed that the fractional settlements provided a more accurate area estimation and spatial distribution, especially for the sites with a small proportion of settlement areas, than the results derived from the per-pixel based approach (See Fig. 8b). This is because per-pixel based approach significantly overestimated the area amount for the pixels with relatively small proportional settlements. Comparative analysis of Figs. 5 and 6 indicated that the regression models based on the human settlement index, or a combination of DMSP-OLS and $NDVI_{max}$ variables, provided better performances in the spatial patterns of human settlement distribution than the regression models based on a single DMSP-OLS or $NDVI_{max}$ variable.

5. Summary and conclusion

Regional or global mapping of human settlements is often based on the DMSP-OLS data with the thresholding technique (Elvidge et al., 1997a; Milesi et al., 2003a). However, different levels of economic development often result in difficulty when selecting suitable thresholds for mapping human settlements (Small et al., 2005). Another challenge for settlement mapping from DMSP-OLS data is the large number of mixed pixels, but previous research has not considered this problem, resulting in loss of spatial information of towns and villages because of their small proportion in a pixel. This paper proposed an integrated approach for estimating fractional settlements through the use of regression models. This approach has proven successful for mapping fractional settlements through the combined use of MODIS $NDVI_{max}$, DMSP-OLS, and ETM+ images. The MODIS and DMSP-OLS can be freely downloaded at the global scale, thus the approach developed in this paper can be used to map human settlements in other regions.

The complementary characteristics between DMSP-OLS and MODIS data made the combined new data sets have more information than each could do individually, as proven in this research. Two

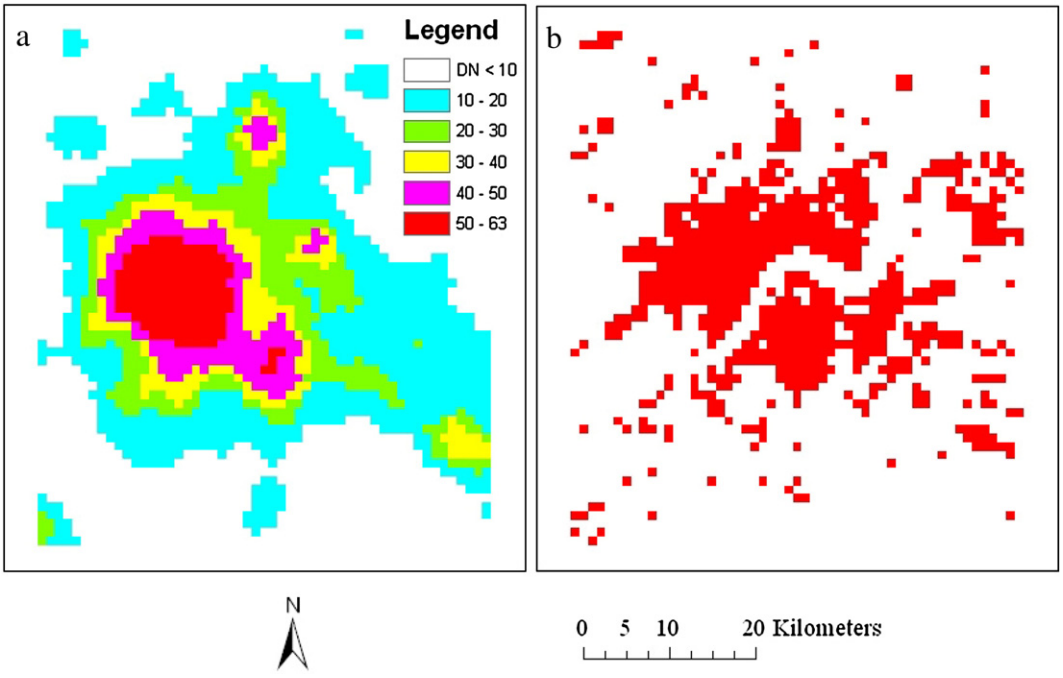

Fig. 8. A comparison of (a) DMSP-OLS data with different data ranges and (b) pixel-based settlement image derived from the human settlement image with a hybrid approach.

methods have been explored in this research. One is to develop a new image called human settlement index based on the integration of both data sources, and the other is to use both data sets as explanatory variables for use in a regression model. Both methods provided a better performance in mapping spatial distribution of settlements than the use of individual DMSP-OLS or MODIS data. More research is needed in the future to explore the potential data fusion approaches for better using multisensor data sources with coarse spatial resolution images in regional and global settlement mapping.

In summary, this research has shown that the combined use of medium and coarse spatial resolution images is promising in settlement mapping at the regional scale. A combination of DMSP-OLS and $NDVI_{max}$ provided a better estimation performance than individual DMSP-OLS or $NDVI_{max}$ variable. The regression models based on either human settlement index or both DMSP-OLS and $NDVI_{max}$ variables greatly improved the spatial patterns of estimated settlement distribution, especially for the sites with small or very high proportional settlements in a pixel. This paper provided a new approach for rapid and accurate estimation of human settlements at the regional scale based on coarse spatial resolution images by combining a limited number of medium spatial resolution images. This research is especially valuable for timely updating human settlement databases at regional and global scales with limited time, labor, and cost.

Acknowledgements

We acknowledge the funding support from NASA Interdisciplinary Science Program (NNG04GM39C) and the Auburn University Peak of Excellence Program, Center for Forest Sustainability. The authors would like to express their thanks to Dr. Silvana Amaral from Instituto Nacional de Pesquisas Espaciais (INPE), Brazil for providing constructive comments and suggestions for revising this paper.

References

Amaral, S., Camara, G., Monteiro, A. M. V., Quintanilha, J. A., & Elvidge, C. D. (2005). Estimating population and energy consumption in Brazilian Amazonia using DMSP night-time satellite data. *Computer, Environment and Urban Systems*, *29*, 179–195.

Amaral, S., Monteiro, A. M. V., Camara, G., & Quintanilha, J. A. (2006). DMSP/OLS night-time imagery for urban population estimates in the Brazilian Amazon. *International Journal of Remote Sensing*, *27*, 855–870.

Ban, Y. (2003). Synergy of multitemporal ERS-1 SAR and Landsat TM data for classification of agricultural crops. *Canadian Journal of Remote Sensing*, *29*, 518–526.

Bauer, M. E., Heinert, N. J., Doyle, J. K., & Yuan, F. (2004). Impervious surface mapping and change monitoring using Landsat remote sensing. *ASPRS annual conference proceedings, May 23–28, 2004, Denver, Colorado* Bethesda, Maryland: American Society for Photogrammetry and Remote Sensing.

Boardman, J. W., Kruse, F. A., & Green, R. O. (1995). Mapping target signatures via partial unmixing of AVIRIS data: In summaries. *Fifth JPL airborne earth science workshopJPL Publication*, *Vol. 1* (pp. 23-26). 95-1.

Bureau of Statistics of China (2006). *China statistical yearbook* (pp. 1031). Beijing: China Statistics Press.

Bureau of Statistics of China (2006). *China City statistical yearbook*. Beijing: China Statistics Press.

Cracknell, A. P. (1998). Synergy in remote sensing — What's in a pixel? *International Journal of Remote Sensing*, *19*, 2025–2047.

Elvidge, C. D., Baugh, K. E., Dietz, J. B., Bland, T., Sutton, P. C., & Kroehl, H. W. (1999). Radiance calibration of DMSP-OLS low-light imaging data of human settlements. *Remote Sensing of Environment*, *68*, 77–88.

Elvidge, C. D., Baugh, K. E., Hobson, V. H., Kihn, E. A., Kroehl, H. W., Davis, E. R., et al. (1997). Satellite inventory of human settlements using nocturnal radiation emissions: A contribution for the global toolchest. *Global Change Biology*, *3*, 387–395.

Elvidge, C. D., Baugh, K. E., Kihn, E. A., Kroehl, H. W., & Davis, E. R. (1997). Mapping of city lights using DMSP Operational Linescan System data. *Photogrammetric Engineering and Remote Sensing*, *63*, 727–734.

Elvidge, C. D., Baugh, K. E., Kihn, E. A., Kroehl, H. W., Davis, E. R., & Davis, C. (1997). Relation between satellite observed visible — Near infrared emissions, population, and energy consumption. *International Journal of Remote Sensing*, *18*, 1373–1379.

Elvidge, C. D., Cinzano, P., Pettit, D. R., Arvesen, J., Sutton, P., Small, C., et al. (2007). The NightSat mission concept. *International Journal of Remote Sensing*, *28*, 3645-2670.

Elvidge, C. D., Imhoff, M. L., Baugh, K. E., Hobson, V. R., Nelson, I., Safran, J., et al. (2001). Night-time lights of the world: 1994–1995. *ISPRS Journal of Photogrammetry and Remote Sensing*, *56*, 81–99.

Fisher, P. (1997). The pixel: A snare and a delusion. *International Journal of Remote Sensing*, *18*, 679–685.

Foley, J. A., DeFries, R., Asner, G. P., Barford, C., Bonan, G., Carpenter, S. R., et al. (2005). Global consequences of land use. *Science*, *309*, 570–574.

Gallo, K. P., Elvidge, C. D., Yang, L., & Reed, B. C. (2004). Trends in night-time city lights and vegetation indices associated with urbanization within the conterminous USA. *International Journal of Remote Sensing*, *20*, 2003–2007.

Gillies, R. R., Box, J. B., Symanzik, J., & Rodemaker, E. J. (2003). Effects of urbanization on the aquatic fauna of the Line Creek watershed, Atlanta — A satellite perspective. *Remote Sensing of Environment*, *86*, 411–422.

Goldewijk, K. K., & Ramnakutty, N. (2004). Land-cover change over the last three centuries due to human activities: The availability of new global data sets. *GeoJournal*, *61*, 335–344.

Haack, B. N., Solomon, E. K., Bechdol, M. A., & Herold, N. D. (2002). Radar and optical data comparison/integration for urban delineation: A case study. *Photogrammetric Engineering and Remote Sensing*, *68*, 1289–1296.

Henderson, M., Yeh, E. T., Gong, P., Elvidge, C., & Baugh, K. (2003). Validation of urban boundaries derived from global night-time satellite imagery. *International Journal of Remote Sensing*, *24*, 595–609.

Imhoff, M. L., Lawrence, W. T., Elvidge, C., Paul, T., Levine, E., Prevalsky, M., et al. (1997). Using nighttime DMSP/OLS images of city lights to estimate the impact of urban land use on soil resources in the U.S. *Remote Sensing of Environment*, *59*, 105–117.

Imhoff, M. L., Lawrence, W. T., Stutzer, D. C., & Elvidge, C. D. (1997). A technique for using composite DMSP/OLS "City Lights" satellite data to accurately map urban areas. *Remote Sensing of Environment*, *61*, 361–370.

Justice, C. O., Townshend, J. R. G., Vermote, E. F., Masuoka, E., Wolfe, R. E., Saleous, N., et al. (2002). An overview of MODIS Land data processing and product status. *Remote Sensing of Environment*, *83*, 3–15.

Kaufmann, R. K., Seto, K. C., Schneider, A., Liu, Z., Zhou, L., & Wang, W. (2007). Climate response to rapid urban growth: evidence of a human-induced precipitation deficit. *Journal of Climate*, 2299–2306.

Lawrence, W. T., Imhoff, M. L., Kerle, N., & Stutzer, D. (2002). Quantifying urban land use and impact on soils in Egypt using diurnal satellite imagery of the Earth surface. *International Journal of Remote Sensing*, *23*, 3921–3937.

Liu, J., Liu, M., Tian, H., Zhuang, D., Zhang, Z., Zhang, W., et al. (2005). Spatial and temporal patterns of China's cropland during 1990–2000: An analysis based on Landsat TM data. *Remote Sensing of Environment*, *98*, 442–456.

Liu, J., Tian, H., Liu, M., Zhuang, D., Melillo, J. M., & Zhang, Z. (2005). China's changing landscape during the 1990s: Large-scale land transformations estimated with satellite data. *Geophysical Research Letter*, *32*, L02405. doi:10.1029/2004GL021649

Lo, C. P. (2001). Modeling the population of China using DMSP Operational Linescan System nighttime data. *Photogrammetric Engineering and Remote Sensing*, *67*, 1037–1047.

Lo, C. P. (2002). Urban indicators of China from DN-calibrated digital DMSP-OLS nighttime images. *Annals of the Association of American Geographers*, *92*, 225–240.

Lu, D., & Weng, Q. (2004). Spectral mixture analysis of the urban landscapes in Indianapolis with Landsat ETM+ imagery. *Photogrammetric Engineering and Remote Sensing*, *70*, 1053–1062.

Lu, D., & Weng, Q. (2005). Urban classification using full spectral information of Landsat ETM+ imagery in Marion county, Indiana. *Photogrammetric Engineering and Remote Sensing*, *71*, 1275–1284.

Lu, D., & Weng, Q. (2006). Use of impervious surface in urban land use classification. *Remote Sensing of Environment*, *102*, 146–160.

Lu, D., & Weng, Q. (2007). A survey of image classification methods and techniques for improving classification performance. *International Journal of Remote Sensing*, *28*, 823–870.

Meyer, W. B., & Turner, B. L., II (1992). Human population growth and global land-use/cover change. *Annual Review of Ecology and Systematics*, *23*, 39–61.

Milesi, C., Elvidge, C. D., Nemani, R. R., & Running, S. W. (2003). Assessing the environmental impacts of human settlements using satellite data. *Management of Environmental Quality*, *14*, 99–107.

Milesi, C., Elvidge, C. D., Nemani, R. R., & Running, S. W. (2003). Assessing the impacts of urban land development on net primary productivity in the southeastern United States. *Remote Sensing of Environment*, *86*, 401–410.

Owen, T. W., Gallo, K. P., Elvidge, C. D., & Baugh, K. E. (1998). Using DMSP-OLS light frequency data to categorize urban environments associated with US climate observing station. *International Journal of Remote Sensing*, *19*, 3451–3456.

Pauleit, S., Ennos, R., & Golding, Y. (2005). Modeling the environmental impacts of urban land use and land cover change — A study in Merseyside, UK. *Landscape and Urban Planning*, *71*, 295–310.

Pickett, S. T. A., Cadenasso, M. L., Grove, J. M., Nilon, S. H., Pouyat, R. V., Zipperer, W. C., et al. (2001). Urban ecological systems: Linking terrestrial ecological, physical, and socioeconomic components of metropolitan areas. *Annual Review of Ecology and Systematics*, *32*, 127–157.

Powell, R. L., Roberts, D. A., Dennison, P. E., & Hess, L. L. (2007). Sub-pixel mapping of urban land cover using multiple endmember spectral mixture analysis: Manaus, Brazil. *Remote Sensing of Environment*, *106*, 253–267.

Ridd, M. K., & Hipple, J. M. (2006). Remote sensing of human settlements. 3rd ed. *Manual of Remote Sensing*, *Vol. 5* (pp. 752). Bethesda, Maryland: American Society of Photogrammetry and Remote Sensing.

Small, C., Pozzi, F., & Elvidge, C. D. (2005). Spatial analysis of global urban extent from DMSP-OLS nighttime lights. *Remote Sensing of Environment*, *96*, 277–291.

Sudhira, H. S., Ramachandra, T. V., & Jagadish, K. S. (2004). Urban sprawl: Metrics, dynamics and modeling using GIS. *International Journal of Applied Earth Observation and Geoinformation*, *5*, 29–39.

Sutton, P. (2003). A scale-adjusted measure of "urban sprawl" using nighttime satellite imagery. *Remote Sensing of Environment*, *86*, 353–369.

Sutton, P., Roberts, D., Elvidge, C., & Baugh, K. (2001). Census from heaven: An estimate of the global population using night-time satellite imagery. *International Journal of Remote Sensing*, *22*, 3061–3076.

Sutton, P., Roberts, D., Elvidge, C., & Meij, H. (1997). A comparison of nighttime satellite imagery and population density for the continental United States. *Photogrammetric Engineering and Remote Sensing*, *63*, 1303–1313.

Welch, R. (1980). Monitoring urban population and energy utilization patterns from satellite data. *Remote Sensing of Environment*, *9*, 1–9.

Weng, Q., Lu, D., & Schubring, J. (2004). Estimation of land surface temperature–vegetation abundance relationship for urban heat island studies. *Remote Sensing of Environment*, *89*, 467–483.

Wu, C., & Murray, A. T. (2003). Estimating impervious surface distribution by spectral mixture analysis. *Remote Sensing of Environment*, *84*, 493–505.

Yang, L., Xian, G., Klaver, J. M., & Deal, B. (2003). Urban land cover change detection through sub-pixel imperviousness mapping using remotely sensed data. *Photogrammetric Engineering & Remote Sensing*, *69*, 1003–1010.

Yocky, D. A. (1996). Multiresolution wavelet decomposition image merger of Landsat Thematic Mapper and SPOT panchromatic data. *Photogrammetric Engineering and Remote Sensing*, *62*, 1067–1074.

Zhou, L., Dickinson, R. E., Tian, Y., Fang, J., Li, Q., Kaufmann, R. K., et al. (2004). Evidence for a significant urbanization effect on climate in China. *PNAS*, *101*, 9540–9544.